Electronic structure of mixed-valence and charge-ordered Sm and Eu pnictides and chalcogenides

V. N. Antonov,[1,*] B. N. Harmon,[1] and A. N. Yaresko[2]
[1]*Ames Laboratory, Iowa State University, Iowa 50011*
[2]*Max Planck Institute for the Physics of Complex Systems, D-01187 Dresden, Germany*
(Received 18 April 2005; published 15 August 2005)

The electronic structure of the mixed-valence Sm and Eu pnictides R_4X_3 (R=Sm, Eu; X=As, Sb, Bi) and samarium and europium chalcogenides Sm_3X_4 (X=S, Se, Te), Eu_3S_4 were investigated theoretically from first principles, using the fully relativistic Dirac LMTO band structure method. The electronic structure is obtained with the rotationally invariant LSDA+U method. We find in Sm_4Bi_3 as a generic feature a very rigid pinning of the energy of Sm $4f$ hole states close to the top of the pnictide p band and the Fermi level pinned to those hole states. Eu_4Bi_3 was found to be a semimetal with low density of states at the Fermi level. The main trends in the electronic structure of the sequence of Sm_4X_3 and Eu_4X_3 compounds (X=As, Sb, or Bi) are discussed. A detailed comparison of the electronic and magnetic structures of Sm_3S_4 and Eu_3S_4 compounds is also presented.

DOI: 10.1103/PhysRevB.72.085119 PACS number(s): 71.28.+d, 71.20.Eh, 75.30.Mb

I. INTRODUCTION

In rare earth compounds, where $4f$ levels are relatively close to the Fermi energy, various anomalous phenomena frequently appear. Most of them can be attributed to the hybridization between the $4f$ states and conduction bands. A mixed-valence (MV) state is one of these phenomena. The MV phenomenon has attracted a great deal of interest during the last several decades in connection with valence fluctuations.[1–5]

In the gas phase most rare earths are divalent, but in the solid state most are trivalent, due to the large cohesive energy gained by promoting a $4f$ electron into an extended bonding state. The rare earth compounds based on Sm, Eu, Tm, and Yb ions frequently exhibit a mixed-valence state consisting of divalent and trivalent valences. In the mixed-valence compounds, therefore, one must also consider the charge degrees of freedom of the $4f$ ions in addition to the spin and orbital degrees of freedom.

To specify this process it is necessary to distinguish between *homogeneously* mixed-valence compounds and *inhomogeneously* mixed-valence compounds. In the former, all the rare earth ions occupy crystallographically equivalent sites and therefore, this is essentially a single ion property where the magnetic ion hybridizes with the sea of the conduction electrons, causing an exchange of the inner $4f$ electron with the conduction band at the Fermi level. Such effects are expected to arise in systems where two electron configurations corresponding to $4f$ occupation numbers n and $n-1$ have nearly degenerate energies. So the ground state of a homogeneously mixed valence compound is a quantum mechanical mixture of both the $4f^n$ and the $4f^{n-1}d$ configuration on each rare earth ion. Typical compounds exhibiting homogeneously mixed-valence phenomena are rare earth materials TmSe, SmS (high pressure golden phase), SmB_6, YbB_{12}, and $YbInCu_4$. The electronic structure of these compounds have been reported in detail in Refs. 6–9, respectively.

In the case of inhomogeneously or static mixed-valence compounds rare earth ions with different valency occupy clearly different sites. However, at high temperatures they become homogeneously mixed-valence semimetals or valence-fluctuating insulators. Their $4f$ electrons are strongly correlated and close to localization, i.e., having a low effective kinetic energy. The $4f$ electrons can hop between the magnetic ions with different valence due to thermal activation (a thermal valence fluctuating state). If the intersite Coulomb repulsion is large enough it may dominate the kinetic energy and, once the charge-disorder entropy due to hopping is low enough, lead to a charge-ordered transition at a critical temperature T_{co} below which the valence fluctuation are suppressed. The resulting inhomogeneously mixed-valence state consists of two species of ions with the $4f^n$ and the $4f^{n-1}d$ configurations. This transition may be compared to a Wigner crystallization on a lattice,[10] and its earliest example is the Verwey transition in magnetite Fe_3O_4,[11] although this picture turned out to be too simplified for this compound.[12,13]

There are several charge-fluctuating inhomogeneous mixed-valence compounds containing rare earth ions. They are the rare earth pnictides Yb_4As_3, Sm_4Bi_3 and Eu_4As_3 with the cubic anti-Th_3P_4 structure and rare earth chalcogenides Sm_3X_4 (X=S, Se or Te) and Eu_3S_4 with the Th_3P_4 structure.

Cubic Sm_4Bi_3 with the anti-Th_3P_4 structure undergoes a first-order transition into a trigonal $R3c$ phase at about 260 K. This change has been ascribed to a charge-ordering transition from the thermal valence fluctuating state into a static mixture of di- and trivalent sites as one of the diagonals of the cube shrinks by approximately 1.4%.[14–17] In charge ordered Sm_4Bi_3, smaller Sm^{3+} ions occupy the short chains.[17] Similar to Yb_4As_3, each magnetic Sm^{3+} chain is isolated from other Sm^{3+} chains by Sm^{2+} ions for which the total angular momentum (J) equals zero. However Sm_4Bi_3 shows a three-dimensional antiferromagnetic order at 2.7 K (Ref. 18) as opposed to Yb_4As_3, where a one-dimensional antiferromagnetic coupling at low temperatures has been predicted[19] and later discovered.[20] At this point, it is of great interest to characterize the nature of the phase transition occurring in Sm_4Bi_3, because the physical properties of its distorted phase have been found to differ from those of Yb_4As_3.

In particular, no maximum occurs in the temperature dependence of the electrical resistivity, nor is there any appreciable linear term in its electronic specific heat.

Contrary to Sm_4Bi_3, two other samarium pnictides Sm_4As_3 and Sm_4Sb_3 show no evidence of charge ordering in a wide temperature range.[15] The change of the character of charge ordering in Sm_4Bi_3 due to pressure has been studied in Refs. 15 and 21. With increasing pressure the resistivity anomaly at the charge ordering transition moves to lower temperatures, becomes weaker, and completely disappears at 2.8 GPa. Above that pressure the crystal undergoes a first-order, isostructural phase transition characterized by an abrupt decrease of the resistance by a factor of 3 and a volume by about 10%. The behavior of the electrical resistivity in the high pressure phase (at 3 GPa) of Sm_4Bi_3 is similar to that of Sm_4As_3 and Sm_4Sb_3.[15] The effect of high pressure can be reproduced by substitution of Bi atoms by smaller Sb atoms. Such an investigation has been reported in Ref. 22. It was found that with increasing Sb content in the $Sm_4(Bi_{1-x}Sb_x)_3$ system, the carrier concentration decreases and the charge ordering temperature slightly increases, while by applying pressure the ordering temperature decreases. This relationship between the substitution and pressure effect in Sm_4Bi_3 is very similar to that in Yb_4As_3. So, it was suggested that Sm_4Bi_3 is a semimetal in the same way as Yb_4As_3. Although the substitution effect may be different from the pressure effect both effects finally lead to enhancement of the Sm^{3+} state relative to Sm^{2+} state. The electronic states of Sm_4As_3 and Sm_4Bi_3 were studied with photoemission spectroscopy in Refs. 23 and 24.

Recently experimental evidence for charge ordering in Eu_4As_3 has been reported. A first following from this result is the observation of trigonal distortion with $a=9.176$ Å, $\alpha=90.855°$, which would indicate a periodic arrangement of the Eu^{2+} and Eu^{3+} ions.[25] Important information concerning the charge ordering of Eu_4As_3 was given by Mössbauer spectroscopy measurements done by Wortman *et al.*[26] They found two absorption peaks separated clearly below $T=340$ K corresponding to the di- and trivalent Eu ions. Above 340 K, these two peaks suddenly unite and the linewidth narrows with increasing temperature. Therefore they concluded that Eu_4As_3 is a thermal valence-fluctuating compound which goes into a charge ordered state below 340 K. Discontinuous changes corresponding to the structural transition are observed in the magnetic susceptibility, too.[18] However, the change of the magnetic susceptibility of Eu_4As_3 at the structural transition temperature is opposite to that of Yb_4As_3, i.e., the magnetic susceptibility of Yb_4As_3 is larger in the low temperature phase, while that of Eu_4As_3 is smaller. The temperature dependence of the specific heat of Eu_4As_3 shows that at the structural transition temperature, a sharp δ-like peak is observed.[18] This indicates that the structural transition is of first order. Eu_4As_3 orders ferromagnetically at $T=18$ K in contrast to Yb_4As_3 and Sm_4Bi_3 which possess antiferromagnetic order at low temperatures. Anomalies in the structural, transport, and thermal properties in Eu_4As_3 associated with this transition are similar to those found in Yb_4As_3 and Sm_4Bi_3.

The samarium chalcogenides Sm_3X_4 (X=S, Se or Te) with the cubic Th_3P_4 structure are well known as typical examples of valence-fluctuation compounds, where two different valence ions, Sm^{2+} and Sm^{3+}, coexist.[27] Such a possibility was mentioned already in the early work of Picon *et al.*[28] He noted that the lattice constants of Sm_3S_4 and Eu_3S_4 are too large in comparison with those of the trivalent $R_3^{3+}S_4$ compounds, indicating that cations with two different valence states 2+ and 3+ coexist in a ratio of 1:2.

Unlike most other Th_3P_4-type rare earth chalcogenides, which are trivalent and metallic,[29] the Sm_3X_4 compounds behave as semiconductors, with a room-temperature electrical resistivity already of the order of 1Ω cm. The activation-type temperature dependence of the dc resistivity $\rho=\rho_0 \exp(E/k_BT)$ has a unique value of the activation energy $E\approx 0.14$ eV for Sm_3X_4 (X=S, Se or Te).[30,31] The optical measurements reveal a direct energy gap in Sm_3S_4 and Eu_3S_4 equal to 0.2 eV and 1.7 eV, respectively.[32,33] The analysis for the dielectric response confirmed that Sm_3Se_4 is a insulator, that is, without free carriers at low temperature.[34] But the gap is so small that it is easily smeared by imperfections like in La doped SmB_6.[15] From x-ray diffraction experiments,[27] both types of Sm ion were found to occupy the same crystallographic site. The magnetic susceptibility of Sm_3X_4 is explained by a sum of the susceptibility of the Van Vleck term for Sm^{2+} with $J=0$ (0 K) and $J=1$ (400 K), and of the Curie term for Sm^{3+} with $J=\frac{5}{2}$ in the coexistence ratio 1:2.[35] Assuming ideal stoichiometry, simple charge balance for the nominal formula $Sm^{2+}(Sm^{3+})_2(X^{2-})_4$ implies that no free carriers are available to populate the conduction band, which explains the lack of metallic conduction observed experimentally. Thermally activated electrical transport takes place, however, through the hopping of electrons among the rare-earth sites.[36] Thus, near room temperature, the Sm ions fluctuate rapidly between two configurations $4f^5$ and $4f^6$, giving rise to the so-called "thermal valence fluctuations." This mechanism differs markedly from the "quantum valence fluctuations" occurring in homogeneously mixed-valence compounds.[1–3,5] Here, the fluctuations slow down drastically as T decreases, as evidenced by the upswing in the transverse nuclear relaxation rate $1/T_2$ on cooling below 160 K (Ref. 37) or the frequency-dependent stiffening of the elastic constants,[38] and an activation-type temperature dependence of the relaxation time, $\tau=\tau_0 \exp(E/k_BT)$. The relaxation time corresponding to the hopping rate in the thermal motion of the $4f$ electron from Sm^{2+} to neighboring Sm^{3+} ions in Sm_3X_4 becomes longer and longer on lowering the temperature, however no sign of a phase transition to a charge-ordered state has been found. In lowering the temperature, the fluctuation of the $4f$ electrons freezes gradually into a charge glass state, which is characterized by the random distribution of Sm^{2+} and Sm^{3+} ions in space. In fact, it has been reported that the broad peaks of the magnetic susceptibility and specific heat around $T_{sg}=1.3$ K in Sm_3Te_4 occur at the transition into the spin-glass state because of the random ordering of the magnetic moments of Sm^{2+} and Sm^{3+} ions.[39]

This result is in contrast with the low-temperature properties of the isomorphic Eu_3S_4 compound. This compound possesses a first order phase transition near $T_{co}=186$ K.[40] The transition exhibits the configurational entropy of an order-disorder transition. The structural changes at the phase

transition of Eu_3S_4 were found to be very small compared, for example, to those of the second-order structural phase transition in La_3S_4.[40] The carrier concentration drops by roughly 3 orders of magnitude in Eu_3S_4 upon cooling below T_{co}.[41] Eu_3S_4 has also a phase transition to a ferromagnetic state below $T_c=3.8$ K.[42] A recent synchrotron x-ray diffraction study for single crystals of Eu_3S_4 has revealed that a Th_3P_4-type $I\bar{4}3d$ structure transforms to a charge-ordered $I\bar{4}2d$ one at $T_{co}=188.5$ K.[43] In the $I\bar{4}2d$ crystal structure all Eu^{2+} ions mix with half the Eu^{3+} in the 8*d* sites and the remaining Eu^{3+} ions occupy the 4*a* sites.

No such effect has been observed in the Sm chalcogenides down to temperatures of less than 1 K. This intriguing result has raised interesting speculations as to the nature of the low-temperature state in the Sm_3X_4 compounds.[44] From the ac conductivity, it has been suggested that, as thermal fluctuations die out at low temperatures, tunneling of 4*f* electrons between neighboring sites may become the dominant transport mechanism. It is known that the tunnel motion of the 4*f* electrons is relevant when the initial and final states possess nearly equal energies.[5] Various spectroscopic probes (Mössbauer effect,[45] NMR,[37] μSR[46]) have been used to determine the charge and magnetic response of these compounds with different characteristic time scales. It now seems most likely that, in Sm_3X_4, the Sm^{3+} moments freeze at low temperature into a spin-glass state,[37,39] possibly associated with a static, or quasistatic, spatial disorder of the two 4*f* configurations. According to this interpretation, the huge linear term, $\gamma=0.6$ J K^{-2}/mol and $\gamma=0.79$ J K^{-2}/mol, observed in the low-temperature specific heat in Sm_3Te_4 and Sm_3Se_4, respectively,[47] can be ascribed to magnetic disorder rather than to heavy-fermion phenomena as proposed initially.

Why does Sm_3X_4 favor the charge glass state and does not exhibit charge ordering with the usual first-order transition with symmetry-breaking character like Eu_3S_4 or Yb_4As_3? To answer this question the microscopic details about the 4*f*-electron states and their degree of hybridization with conduction states are highly relevant.

The aim of the present study is to explore the electronic structures of some mixed-valence Sm and Eu chalcogenides and pnictides with Th_3P_4 and anti-Th_3P_4 structures, namely, Eu_3S_4, Sm_3X_4 (X=S, Se, and Te) and R_4X_3 (R=Sm, Eu; X=As, Sb, and Bi) compounds.

The paper is organized as follows. Section II presents a description of Th_3P_4 and anti-Th_3P_4 crystal structures and the computational details. Section III is devoted to the electronic structure of Sm and Eu pnictides R_4X_3 (R=Sm, Eu; X=As Sb, Bi). Section IV is devoted to the electronic structure of Sm_3X_4 (X=S, Se, and Te) and Eu_3S_4 compounds calculated in the LSDA+U approximation. Finally, the results are summarized in Sec. V.

II. CRYSTAL STRUCTURE AND COMPUTATIONAL DETAILS

The high-temperature phases of R_4X_3 (R=Sm, Eu; X=As Sb, Bi) compounds have the cubic anti-Th_3P_4 structure with space group $I\bar{4}3d$ (No. 220). The R ions occupy the P-sites with Wyckoff positions 16*c* ($x=y=z=u$), and the X ions occupy the Th sites with special Wyckoff positions 12*a* ($x=3/8$, $y=0$, $z=1/4$).[48] All R atoms are aligned on four families of chains oriented along the four diagonals of the cubic unit cell.[49]

The high-temperature phases of Eu_3S_4 and Sm_3X_4 (X=S, Se or Te) compounds have the bcc Th_3P_4 structure with space group $I\bar{4}3d$ (No. 220). Conventional unit cell of Eu_3S_4 includes four formula units. Both ions Eu^{2+} and Eu^{3+} in Eu_3S_4 occupy crystallographically equivalent 12*a* sites ($x=3/8$, $y=0$, $z=1/8$) with S_4 symmetry. S occupies the 16*c* sites ($x=y=z=u$). Only the x coordinate of sulfur (u parameter) is a variable among positional parameters. We used the experimentally determined values of $u=0.0721$, 0.0722, 0.0724, 0.0724 for Eu_3S_4, Sm_3S_4, Sm_3Se_4, and Sm_3Te_4, respectively.[48] It gives a slight deviation from an ideal Th_3P_4 structure ($u=1/12=0.0833$). A Eu ion is coordinated by eight sulfur ions in a distorted cube while a sulfur ion is coordinated by six Eu ions.

A recent synchrotron x-ray diffraction study for single crystals of Eu_3S_4 has revealed that a low temperature charge-ordered structure with tetrahedral symmetry and a space group of $I\bar{4}2d$ (No. 122). The cell dimensions are $a=8.508$ Å and $c=8.514$ Å.[43] Eu ions occupy crystallographically two nonequivalent positions, namely, 4*a* ($x=y=z=0$) and 8*d* ($x=3/8$, $y=1/4$, $z=1/8$) sites. S ions occupy the 16*e* sites ($x=0.572$, $y=0.823$, $z=0.449$).[43] Both Eu sites are coordinated by eight sulfur ions. The 4*a* sites are distributed as in the diamond structure. The mean Eu-S distance for the 8*d* sites is about 0.3% larger than for the 4*a* sites.

The details of the computational method are described in our previous papers,[6–8] and here we only mention several aspects. The calculations were performed for the experimentally observed lattice constants $a=8.822$, 9.308, 9.815 Å for Sm_4X_3 and $a=9.192$, 9.654, 10.00 Å for Eu_4X_3 (X=As, Sb, and Bi), respectively; $a=8.523$ Å for Sm_3S_4, 8.877 Å for Sm_3Se_4 9.511 Å for Sm_3Te_4, and 8.527Å for Eu_3S_4. We used the spin-polarized fully relativistic linear-muffin-tin-orbital (SPR LMTO) method[50,51] in the atomic sphere approximation (ASA) with the combined correction term taken into account. The LSDA part of the calculations was based on the spin-density functional with the von Barth-Hedin parametrization[52] of the exchange-correlation potential. Brillouin zone (BZ) integrations were performed using the improved tetrahedron method[53] and charge self-consistency was obtained on a grid of 262 irreducible **k** points for Sm and Eu chalcogenides and 252 and 924 **k** points of the cubic and the trigonal Sm and Eu pnictides, respectively. To improve the potential we include an additional empty sphere in the (1/4, −1/8, 0) position for the Sm and Eu pnictides, the corresponding empty spheres in rare earth chalcogenides have been placed in the (1/4, 1/8, −1/2) and (0, 1/4, −1/8) positions. The basis consisted of rare earth *s*, *p*, *d*, and *f*; chalcogenide and pnictide *s*, *p*, *d*, and empty sphere *s* and *p* LMTO's.

We also neglect the small trigonal distortion in Sm pnictides for simplicity and determined all positions in such a

way that there is no ion displacement at all in the cubic to trigonal transformation, rather the rare earth f-charges are redistributed by fixing which rare earth site is 3+ and which is 2+. We checked that this neglect of ion displacements makes very little differences in our results. It should be mentioned that if we neglect the trigonal distortion, the LSDA (without U) band structure calculations should give exactly the same results as for the cubic structure.

We have adopted the LSDA+U method[54] as a more appropriate approximation to treat the electron-electron correlation. We used the "relativistic" generalization of the LSDA+U method which takes into account spin-orbit coupling so that the occupation matrix of localized electrons becomes nondiagonal in spin indexes. This method is described in detail in our previous paper[55] including the procedure to calculate the screened Coulomb U and exchange J integrals, as well as the Slater integrals F^2, F^4, and F^6.

Screened Coulomb U and exchange J integrals enter the LSDA+U energy functional as external parameters and have to be determined independently. Their values can be obtained from LSDA calculations using Slater's transition-state approach as described in Ref. 56. For Sm_4X_3 compounds such calculations give the values of U=7.2, 7.14, and 7.0 eV for X=As, Sb and Bi, respectively. For Eu_4X_3 compounds we obtain the values of U=7.47, 7.35, and 7.25 eV for X=As, Sb, and Bi, respectively. For Sm_3X_4 compounds U=8.2, 8.2, and 8.5 eV for X=S, Se, and Te, respectively. For Eu_3S_4 U=8.3. The exchange parameter is taken as J=0.62 eV for Sm_4As_3 and 0.65 eV for all other rare earth pnictides. For Sm chalcogenides J=0.65 eV and 0.67 eV for Eu_3S_4.

III. SAMARIUM AND EUROPIUM PNICTIDES

A. Sm_4Bi_3

It is well known that the application of plain LSDA calculations to 4f-electron systems is often inappropriate, because of the correlated nature of the 4f shell.[4] The position of the LSDA 4f states close to the Fermi energy is in contradiction to the findings of XPS and UPS experiments.[3,4] To account better for the on-site f-electron correlations, we have adopted as a suitable model the LSDA+U approach.[55]

The LSDA+U partial DOS's of antiferromagnetic (AF) Sm_4Bi_3 are shown in Fig. 1. In order to imitate the nonmagnetic (J=0) ground state of Sm^{2+} ion the exchange-correlation potential is taken to be the same for both spin states within the corresponding atomic spheres. For three divalent nonmagnetic Sm ions six $4f_{5/2}$ energy bands per ion are fully occupied and hybridize with Bi p states at around −2.0 eV below Fermi energy. The other eight $4f_{7/2}$ divalent Sm energy bands are situated far above the Fermi level at 6.5 eV and hybridize with Sm 5d states. Both, the occupied and empty $Sm^{2+}4f$ states are very narrow which indicates that their hybridization with Bi p and Sm d states is rather weak. For the trivalent Sm ion, seven spin-down 4f electron bands per ion are well above the Fermi level and hybridize with Sm 5d states. Five spin-up $Sm^{3+}4f$ states are below the Fermi level situated right in the energy gap between Bi s and p states (not shown). The other two spin-up 4f energy bands

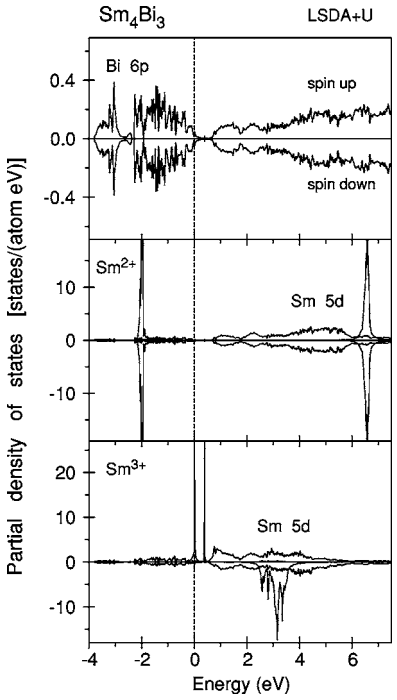

FIG. 1. The partial density of states [in states/(atom eV)] of Sm_4Bi_3 calculated in LSDA+U approximation (U=7.0 eV) for the low temperature $R3c$ phase.

for the trivalent Sm ion, doubly degenerate due to AF ordering, appear just below the top of the Bi p band. One of them is completely empty and above the Fermi energy at around 0.15 eV, but the other one is pinned to the Fermi level. The sixth and seventh 4f spin-up energy bands have different orbital character, m_j=−5/2 and m_j−=7/2, respectively, and their splitting is mainly caused by the nonspherical part of the Coulomb interaction.

The pinning of the sixth spin-up $Sm^{3+}4f$ state to the Fermi level is a robust feature of the electronic structure of the Sm_4Bi_3 compound. As an example, we present in Fig. 2 the energy bands of Sm_4Bi_3 for different values of Coulomb parameter U. The sixth spin-up $Sm^{3+}4f$ state just slices near the top of the Bi p band when U is varied from 3 to 10 eV. Only for $U \geqslant 10.5$ eV does the Sm 4f band become empty. Such pinning of the 4f state to the Fermi level may be explained by the charge balance between Sm 4f states of the Sm^{3+} ions and pnictide p states. This feature in combination with the small mass of the Bi p electrons close to the top of the p band appears to be a key point for the physics of the Sm pnictides.

In Fig. 2 for drawing of the 4f bands we used the so-called *fat-bands* representation. The size of the circles indicates the degree of the 4f orbital character in a band. Such a representation can help to visualize also the hybridization between Sm 4f and Bi p states. The largest Sm 4f-Bi p hybridization was found to be near the Γ symmetry point in the Γ-P direction. Due to the very small phase space for hybridization and the very small Sm 4f-Bip orbital overlap, the DOS peak of the sixth hole spin-up 4f band pinned at the Fermi level is as narrow as 0.01 eV.

This situation is similar to that found in the charge ordering of Yb_4As_3 (Ref. 57) where a very narrow marginally

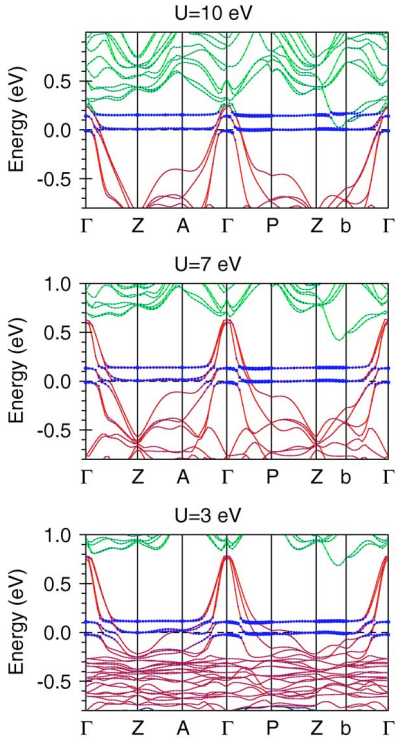

FIG. 2. (Color online) The energy band structure of Sm_4Bi_3 calculated in LSDA+U approximation around the Fermi level for various values of U.

occupied $Yb^{3+}4f$ hole band is also pinned close to the very top of the As p valence band via the charge balance between Yb and As. One should mention, however, that there are also some important differences. There are two $4f$ energy bands crossing the top of the Bi p band in Sm_4Bi_3, but only a single one in the Yb_4As_3 compound. The later case corresponds to a ground state with a hole pocket around the Γ point ($\mathbf{k}=0$) holding 0.0058 As p holes per formula unit. In the case of Sm_4Bi_3 a hole pocket around the Γ-point contains 0.25 Bi p holes per formula unit. As a consequence the carrier concentration is relatively large in Sm_4Bi_3. However, the most prominent difference in the electronic structure of the Sm_4Bi_3 in comparison with the Yb_4As_3 compound is the value of the spin moment of the corresponding magnetic ions. The Yb^{3+} ions occupying short chains in Yb_4As_3 have the $4f^{13}$ configuration with an effective spin of $s=1/2$. This leads to appearance of one-dimensional spin 1/2 chains with antiferromagnetic coupling at low temperatures.[20] The trivalent Sm^{3+} ions with the $4f^5$ configuration have a spin moment $s=5/2$ and Sm_4Bi_3 possesses a three-dimensional antiferromagnetic order.[18] The Fermi surface of Sm_4Bi_3 consists of two closed hole pockets of Bi p states centered at the Γ point and two electron ellipsoids of Sm f states centered at P and A symmetry points. The corresponding Fermi surface of Yb_4As_3 consists of a hole pocket of As p states centered at the Γ point and an electron ellipsoid of Yb f states centered on the symmetry line Γ-P.

The mobility of heavy $4f$ holes is assumed to be negligible in comparison with the mobility of pnictide p electrons. So the transport properties of Sm_4Bi_3 are mostly determined by the number of pnictide p holes.

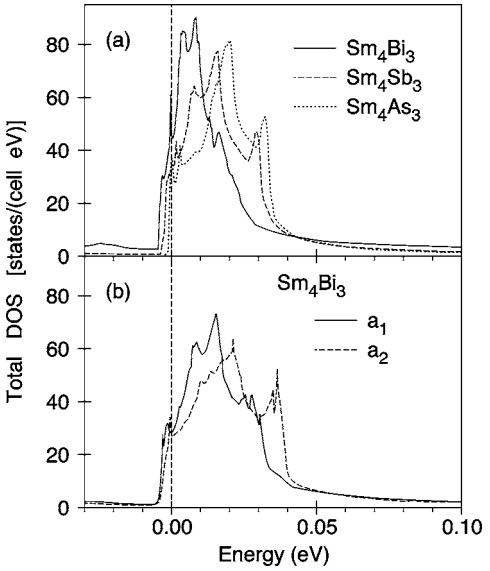

FIG. 3. Expanded view of the DOS of (a) Sm_4X_3 (X=As, Sb, Bi) and (b) Sm_4Bi_3 for the lattice constants a_1=9.308 Å and a_2=9.561 Å.

B. Sm_4As_3 and Sm_4Sb_3

The main trend in the electronic structure of the sequence of Sm_4X_3 compounds (X=As, Sb, or Bi) results from the characteristic trend in the pnictide p wave functions and from the systematic change of the lattice parameters. The counteraction of screening by inner atomic shells and of relativistic effects leads to the characteristic trend in the position of the atomic p state and hence the center of gravity of the pnictide p band decreases from As to Bi. The p bandwidth is monotonically increasing from As to Bi due to the increasing extension of the atomic wave function, although the lattice constant increases too. The degree of pinning of Sm sixth $4f$ spin-up energy band to the Fermi level in Sm_4Sb_3 and Sm_4As_3 is similar to that obtained for the Sm_4Bi_3 compound. An artificial shift via tuning U of the hole f level by changing U by 6 eV is completely compensated by a charge transfer as small as 0.2 electron.

The most prominent difference in the electronic structure of the Sm_4Bi_3 compound in comparison with the other two samarium pnictides is in the position and occupation of the sixth hole $4f$ spin-up energy level. Figure 3(a) shows the expanded view of the total DOS of Sm_4X_3 (X=As, Sb, or Bi) compounds. If one moves from Sm_4Bi_3 to Sm_4As_3 through the series, the peak position of the sixth hole $4f$ spin-up level shifts toward higher energy from the Fermi level. The occupation of the sixth hole $4f$ spin-up level reduces from 0.25 electrons in Sm_4Bi_3 to 0.15 electrons in Sm_4Sb_3 and to 0.01 electrons in Sm_4As_3. Therefore the Sm^{3+} state is enhanced relative to the Sm^{2+} one in the series. This is consistent with the conclusion derived in Ref. 22 on the $Sm_4(Bi_{1-x}Sb_x)_3$ system. We should mention here that when we speak about partial occupation of the sixth f hole level in Sm_4X_3 compounds we imply that such an occupation is due to the hybridization effect between pnictide p and Sm $4f$ energy states.

The Sm_4X_3 pnictides offer the unique opportunity to follow the evolution of intermediate valence as a function of

composition. The driving force is the change of lattice constant upon exchanging the anion. In order to separate the influence of the lattice constant from the influence of the ionic potential of the pnictide component on the electronic structure of Sm_4X_3 (X=As, Sb, and Bi), we present in Fig. 3(b) the DOS of Sm_4Bi_3 evaluated with the lattice constant of Sm_4Sb_3 (a=9.308 Å) and for a=9.561 Å. The peak positions of the sixth hole 4f spin-up level of Sm_4Bi_3 with lattice parameter equal to that of the Sm_4Sb_3 compound and real samarium antimonide are almost the same indicating the major role played by the lattice constant in this case. On the other hand, the occupation number of the sixth hole 4f spin-up level in the compressed Sm_4Bi_3 is 1.5 times larger than in the Sm_4Sb_3 compound. The reason is the larger Sm 4f-pnictide p hybridization in the former case due to larger extension of the atomic Bi 6p wave function in comparison with the Sb 5p one. We can conclude that in the cases of the Sm_4X_3 compounds the type of pnictide ion potential plays an essential role.

The results of the band structure calculations for Sm_4As_3 and Sm_4Sb_3 presented above were obtained with the assumption that the compounds contain three Sm^{2+} and one Sm^{3+} ions in the unit cell similar to Sm_4Bi_3. In this case it is still not clear why Sm_4As_3 and Sm_4Sb_3 show no trace of charge ordering at low temperatures. On the other hand, in earlier work Ochiai *et al.*[15] suggested that Sm_4As_3 and Sm_4Sb_3 are typical dense Kondo systems with all four Sm ions being in the trivalent state. From the volume collapse in the high pressure phase of Sm_4Bi_3 it was deduced that all Sm ions must be close to trivalency in this phase.[14,21]

The electronic structure of Sm_4As_3 with trivalent Sm ions (not shown) differs significantly from the band structure with only one Sm ion in the trivalent state. In the former case As 4p states are completely occupied and are far below the Fermi level. On the other hand, the previously empty Sm 5d states become occupied due to $4f \rightarrow 5d$ charge transfer. A similar band structure was found also in Sm_4Sb_3 with trivalent Sm ions.

Independently of the number of trivalent Sm ions the sixth 4f hole level is always pinned at the Fermi energy. It makes the usual Kondo lattice scenario inappropriate for Sm_4As_3 and Sm_4Sb_3 because for a Kondo resonance to develop, both the occupied and empty 4f states must be sufficiently far away from the Fermi level.

In conclusion we note that the question how many Sm ions are in the trivalent state in Sm_4As_3 and Sm_4Sb_3 compounds as well as in the high pressure phase of Sm_4Bi_3 (above 2.8 GPa) is still open. Analysis of the lattice constants suggests all four Sm ions are probably in the trivalent state.[14,15] On the other hand, the magnetic susceptibility at room temperature in Sm_4As_3 is definitely larger than the theoretical value for Sm^{3+}, which can be explained by over 10% mixing of Sm^{2+}.[15] Moreover, high resolution 4d-4f resonance photoemission spectra of Sm_4As_3 have quite intensive components at 0 to 4 eV binding energy,[3,4] which indicates a significant amount of Sm^{2+} ions in the compound.

The principal question about the degree of Sm valency might be answered also by optical measurements. In Fig. 4 we show the optical reflectivity and conductivity spectra of Sm_4As_3 calculated in the LSDA+U approximation for different Sm valencies. The most prominent difference in the spectra is the extra peak between 0 and 1 eV in the optical conductivity with all four Sm ions in the trivalent state caused by interband transitions involving the occupied 5d hybridized states. In Sm_4As_3 with only one Sm ion being in the trivalent state Sm 5d states are completely empty. As a result, the transitions involving the occupied 5d states do not take place at small photon energies, and the erroneous peak structures around 0 to 1 eV disappear from the optical spectra. A small peak at around 0.15 eV presented in the optical conductivity spectrum with one Sm ion in the trivalent state is mostly determined by the interband transitions involving occupied states with predominantly As p character to unoccupied states with predominantly Sm 4f character situated in close vicinity of the Fermi level. Experimental measurements of the optical spectra in Sm_4As_3 and Sm_4Sb_3 are highly desired.

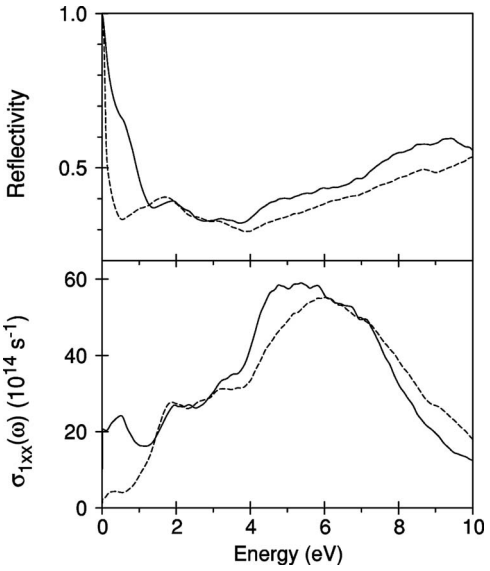

FIG. 4. Calculated optical reflectivity $R(\omega)$ and conductivity $\sigma(\omega)$ in Sm_4As_3 with one (dashed line) and all four Sm ions in the trivalent state (full line).

We should mention that the experimental situation in Sm_4X_3 differs from that, for example, in Yb_4As_3 or Eu_4As_3 in the sense that in the later systems a generation of samples of much better quality became available during recent years, and more reliable data about transport properties, optical and photoemission spectra were obtained. In Sm_4X_3 we still use old experimental data and it is difficult to ascertain the full validity of measured properties based on the experiments of the early 1980s. The physical nature of the mixed valence state in Sm_4As_3 and Sm_4Sb_3 compounds as well as in the high pressure phase of Sm_4Bi_3 requires further investigation theoretically as well as experimentally.

C. Eu_4X_3 (X=As, Sb, and Bi)

Figure 5 shows the energy band structure and total density of states near the Fermi level for Eu_4As_3, Eu_4Sb_3, and Eu_4Bi_3 calculated in the LSDA+U approximation. For divalent ferromagnetic Eu ions seven 4f spin-up energy bands per ion

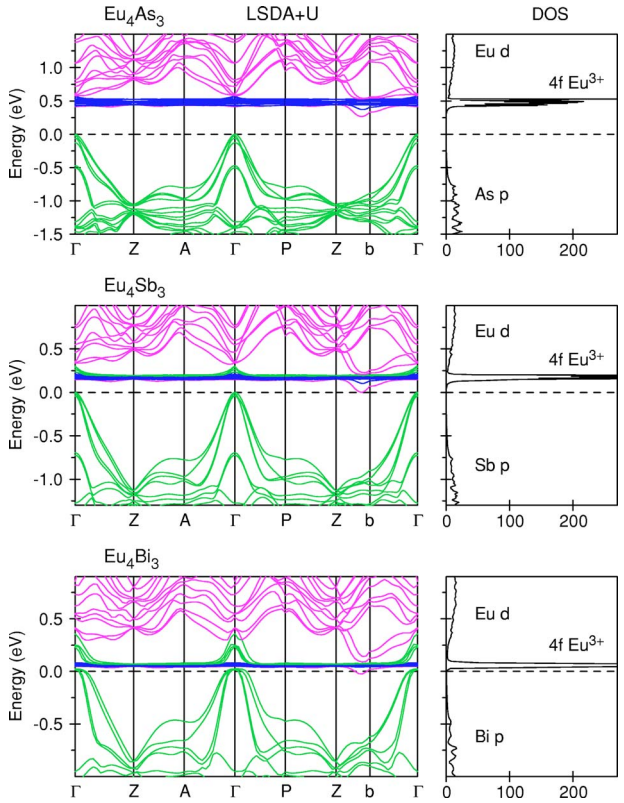

FIG. 5. (Color online) The energy band structure and total DOS [in states/(cell eV)] of Eu_4As_3, Eu_4Sb_3, and Eu_4Bi_3 calculated in LSDA+U approximation (U=7.47, 7.35, and 7.25 eV, respectively).

are fully occupied and hybridize with the bottom of the pnictide p states (not shown). The other seven $4f$ spin-down divalent Eu energy bands are situated far above the Fermi level at 7 to 7.5 eV and are hybridized with Eu $5d$ states. The six $4f_{5/2}Eu^{3+}$ bands are fully occupied and situated in the gap between the pnictide s and p states while eight $4f_{7/2}$ hole levels are completely unoccupied and cross the top of pnictide p band and bottom of the Eu $5d$ band. There is a hybridization energy gap of ΔE=0.05 eV in Eu_4Bi_3 which is formed between Bi p and $Eu^{3+}4f_{7/2}$ states.

The Fermi surface of Eu_4Bi_3 consists of small closed hole pockets of Bi p states centered at the Γ point and an electron ellipsoid of Eu $5d$ states centered at the Z-b symmetry direction. There are no $4f$ states at the Fermi level.

As in the case of Sm_4X_3 the main trend in the electronic structure of the sequence of Eu_4X_3 compounds (X=As, Sb, or Bi) results in a monotonic increase of the p bandwidth going from As to Bi due to an increasing extension of the atomic wave function. Therefore, as one moves from Eu_4Bi_3 to Eu_4As_3 through the series, the unoccupied $4f_{7/2}$ levels for nonmagnetic Eu^{3+} move from below toward the very top of the pnictide p band. If Eu_4Bi_3 is a semimetal, Eu_4As_3 and Eu_4Sb_3 are both semiconductors. The direct gap is equal to 0.41 eV and 0.12 eV and the indirect gap −0.26 eV and 0.02 eV in Eu_4As_3 and Eu_4Sb_3, respectively. These gaps are between pnictide p and Eu $5d$ bands.

The temperature dependence of the Hall coefficient single crystal Eu_4As_3 is presented in Ref. 18. Large values of the Hall coefficient indicate a very low carrier concentration of this system. The same holds true for the electrical resistivity, which is, for instance, estimated as about 0.005 carriers/Eu ion at 200 K, assuming a one band model. Its positive sign suggests dominant hole conductivity in a wide temperature range. On the other hand, from our band structure calculations Eu_4As_3 is a semiconductor. Although the calculated indirect gap is rather small in this system and any crystal imperfections or small doping can easily close the gap.

We should mention that among Eu_4X_3 (X=As, Sb, and Bi) compounds only Eu_4As_3 reveals the charge ordering cubic-to-trigonal structural transformation. There is no information on the charge ordering for the other two compounds in the literature.[58]

IV. SAMARIUM AND EUROPIUM CHALCOGENIDES

A. Density of states

(a) Eu_3S_4: The analysis on the site preference of Eu^{2+} and Eu^{3+} ions presented in Ref. 43 shows that Eu^{2+} ions do not occupy the $4a$ sites within the error estimates. The ionic radii of Eu^{2+} and Eu^{3+} ions are 1.25 and 1.07 Å.[59] Larger Eu^{2+} ions prefer the slightly larger $8d$ sites, although both sites are surrounded by eight sulfur atoms in the coordination of a distorted cube. The ordering scheme is that the Eu^{3+} ions occupy the $4a$ sites, while both Eu^{2+} and Eu^{3+} ions occupy the $8d$ sites in the ratio of 1:1. The chemical formula involving the information on the valence is given as $[Eu^{3+}]_{4a}[Eu^{2+}Eu^{3+}]_{8d}(S^{2-})_4$. Two isomer shift peaks of Mössbauer spectra of Eu_3S_4 supports the separation of Eu^{2+} and Eu^{3+} ions below T=228 K.[60] Since the observation temperature is higher than T_{co}=188.5 K, the gradual freezing of electron hopping occurs independently of the crystal-structural change, where the crystal still maintains the Th_3P_4-type structure. The frequency of hopping can be described as a relaxation time τ to exchange the electrons in the observation of the Mössbauer spectra. Exponential temperature dependence of τ was reported with a continuous change through the phase transition. The τ values are 1.0^{-7}, 3.5^{-8}, 8.5^{-10}, 3.5^{-11} s at T=83, 200, 250, and 325 K, respectively.[60] It should be noted that the hopping of electrons still exists at T=83 K even below the phase-transition temperature of T_{co}=188.5 K. Similar gradual freezing of electron hopping was observed in the neutron and x-ray Huang scattering of magnetite.[61,62]

Although the distribution of Eu^{2+} and Eu^{3+} ions at $8d$ sites is random below T_{co}=188.5 K, the energy barrier to enable the electron hopping is relatively small even in the low-temperature phase so far examined. Therefore a charge ordering between Eu^{2+} and Eu^{3+} ions may exist for Eu_3S_4.[43]

Figure 6 shows the partial density of states of Eu_3S_4 for the low temperature $I\bar{4}2d$ phase calculated in the LSDA+U approximation for $U_{eff}=U-J$=7.63 eV. In our LSDA+U band structure calculations of Eu_3S_4 we assumed an additional charge ordering of the Eu^{2+} and Eu^{3+} ions in $8d$ sublattice (see Fig. 7) in a way which has been done in the case of the low-temperature charge-ordered magnetite Fe_3O_4 in B sublattice for Fe^{2+} and Fe^{3+} ions.[12] In contrast to LSDA,

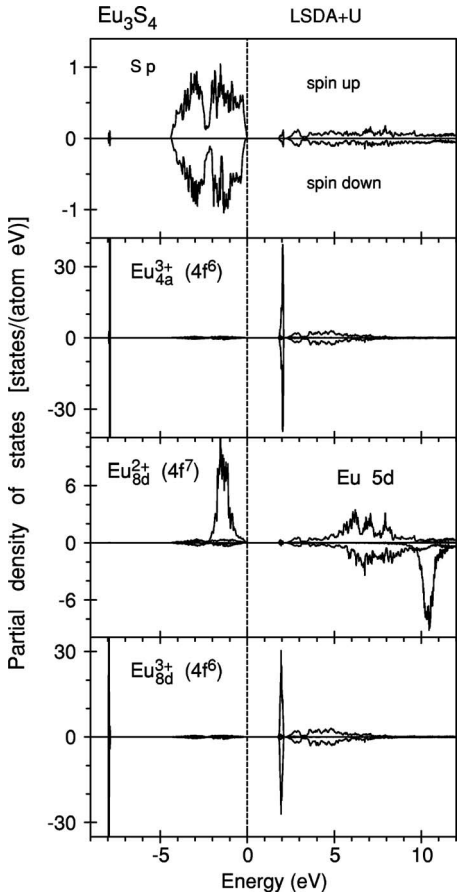

FIG. 6. The partial density of states (DOS) [in states/(atom eV)] of Eu_3S_4 in $I\bar{4}2d$ phase calculated in LSDA+U approximation.

where the stable solution for Eu_3S_4 is metallic, the LSDA+U method gave an insulator consistent with the experimental situation described in the introduction.

For divalent magnetic Eu^{2+}_{8d} ions seven $4f$ spin-down energy bands per ion are situated at the top of Eu $5d$ states at 10 to 11 eV above Fermi level. The $4f$ spin-up energy bands per ion are fully occupied and hybridized with about a half of the S p band. There is a quasienergy gap between hybridized

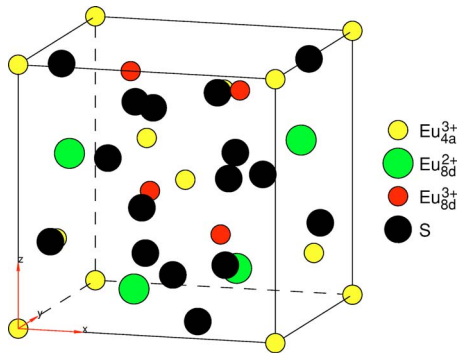

FIG. 7. (Color online) Crystal structure of a low temperature phase of Eu_3S_4. Small white balls, Eu^{3+} ions in the $4a$ crystallographic positions. Large gray balls, Eu^{2+} ions in the $4a$ positions; small dark balls, Eu^{3+} ions in the $4a$ positions. Large black balls, S ions.

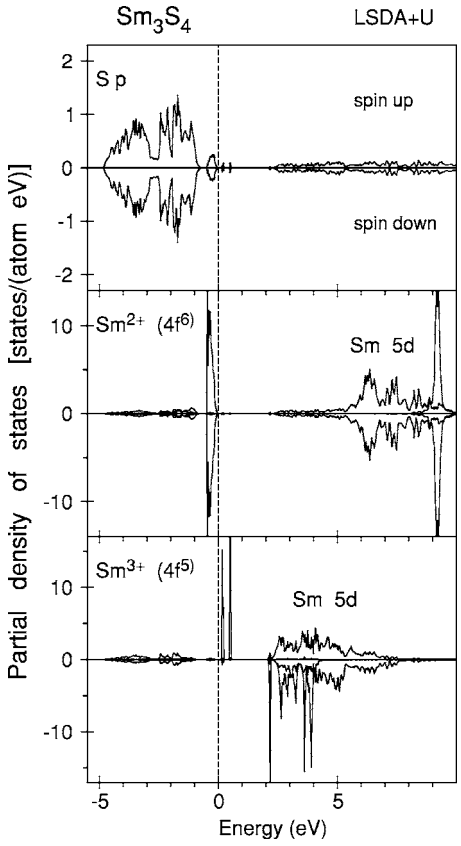

FIG. 8. The partial density of states (DOS) [in states/(atom eV)] of Sm_3S_4 calculated in LSDA+U approximation.

and nonhybridized parts of S p bands at −2.1 to −2.4 eV (Fig. 6). Six $4f_{5/2}Eu^{3+}$ nonmagnetic bands for both the $4a$ and $8d$ sites are fully occupied and situated in the gap between S s and p states, while eight $4f_{7/2}$ hole levels are completely unoccupied and cross the very bottom of the Sm $5d$ states at around 2 eV above the Fermi level (Fig. 6). Both the occupied and empty $4f$ Eu^{3+}_{4a} states are shifted downward at around 0.1 eV in comparison with the position of the $4f$ Eu^{3+}_{8d} states due to slightly different chemical bonding.

(b) Sm_3S_4: The inhomogeneous mixed-valence state on the Sm sublattice was modeled by lowering the crystal symmetry in such a way that $12a$ sites split into two groups consisting of four and eight equivalent sites. The former were occupied by Sm^{2+} and the latter by Sm^{3+} ions.

In contrast to LSDA, where the charge-inhomogeneous solution for Sm_3S_4 is metallic, the LSDA+U method gave an insulator. Sm^{2+} nonmagnetic $4f_{5/2}$ bands are fully occupied and situated at the very top of S p energy band (Fig. 8). The $4f_{7/2}$ hole levels are completely empty and well above the Fermi level hybridized with Sm $5d$ states at around 9 eV (Fig. 8). For trivalent Sm ions seven $4f$ spin-down energy bands per ion are situated above Fermi level at 2.2 to 4.0 eV hybridized with Sm $5d$ states. Five $4f$ spin-up energy bands per ion are fully occupied and situated in the gap between S s and p energy bands (not shown). The other two empty $4f$ spin-up energy bands are situated just above the Fermi level in the gap between occupied nonmagnetic $4f_{5/2}Sm^{2+}$ bands and empty Sm $5d$ bands (Fig. 8).

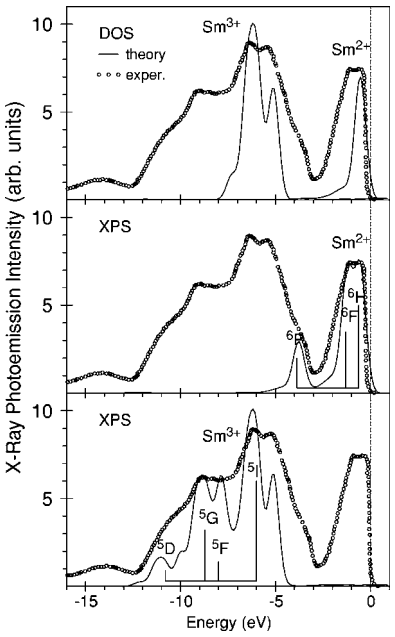

FIG. 9. Comparison of the calculated $4f$ DOS of Sm_3S_4 in the LSDA+U approximations with the experimental XPS spectrum from Ref. 3 taking into account the multiplet structure of the $4f^5$ final state (see explanations in the text).

B. XPS spectra

Photoemission experiments, both x-ray (XPS) and ultraviolet, are of central importance for understanding mixed-valence materials (see the review of the early work by Campagna *et al.*[63]). In rare-earth photoemission, when the photon ejects an electron from the $4f^n$ shell it leaves behind a $4f^{n-1}$ configuration, hence the kinetic energy distribution curve of the emitted electron measures the spectra of the final-state hole. The final state $4f^{n-1}$ has a characteristic multiplet splitting which serves as a fingerprint, and these are accurately resolved and calculable for rare-earth photoemission. By identifying the final-state hole the initial state can be inferred.

The partial $4f$ DOS of the occupied part of the Sm_3S_4 calculated in the LSDA+U approximations is compared with XPS measurements[64] in the top panel of Fig. 9. The calculated $4f$ DOS has been broadened to account for lifetime effects and for experimental resolution. The S $3p$ states essentially do not contribute to the XPS spectra because of the low ionization cross section compared with that of the Sm $4f$ states.[65] Hence, the measurements only indicate the f excitation energies relative to the Fermi level.

The theoretical $4f$ DOS calculated using one electron approximations cannot, of course, fully account for the multiplet splitting. Therefore we present in two other panels of Fig. 9 the $4f$ DOS's taking into account the multiplet structure of Sm^{2+} and Sm^{3+} ions. We used the final state multiplet structure presented in Ref. 66. The multiplet structure for Sm^{2+} ion ($4f^5$ final state) consists of three terms ^{6}H, ^{6}F, and ^{6}P. The Sm^{3+} ion ($4f^4$ final state) has the multiplets ^{5}I, ^{5}F, ^{5}G, and ^{5}D. The relative intensities for the multiplet peaks were obtained on the basis of Cox calculations[67] using the fractional parentage method.[68] In this method the Hund's rule ground state is assumed for n $4f$ electrons and then the coefficients of fractional parentage (Racah's) for the $n-1$ configurations are calculated. The intensities for the various configurations (multiplets) are just the square of the coefficients of fractional parentage. In Fig. 9 the XPS spectrum is modeled by a weighted sum of $4f$ DOS curves. We aligned the centroid of the calculated occupied $4f$ DOS peak with the centroid of the atomic final state multiplet and summed up the spectra scaling them according to the relative intensities of the multiplets. The agreement between LSDA+U theory and the XPS measurements is reasonably good. The disagreement in the intensity of some peaks might be explained by the influence of transition matrix elements which have not been included in the theoretical calculations. It is clear that the structures between −4.5 and −16 eV binding energy should be assigned to the final-state multiplet structure derived from five fully occupied $Sm^{3+}4f$ spin-up bands and the structures between 0.0 and −4.5 eV are associated with the final-state multiplet structure of the divalent $Sm^{2+}4f$ DOS. The LSDA calculations place $4f$ energy bands in close vicinity of the the Fermi level for both the Sm^{2+} and Sm^{3+} ions and hence are not able to produce the structures of the XPS spectrum in the −4.5 to −16 eV eV energy interval.

C. Optical spectra

From the good agreement between theory and XPS measurements we may conclude that the LSDA+U calculations give an accurate position for the occupied $4f$ bands. The principal question is the energy position of the empty $4f$ states, which is usually answered by optical or BIS measurements. Although optical measurements give more precise information on the band positions in comparison with XPS measurements due to much better resolution, they involve complex functions containing information of both the initial and final states simultaneously (joint density of states) and are strongly influenced by the optical transition matrix elements.

In Fig. 10 we show the experimental[32] real refractive index $n(\omega)$, extinction coefficient $k(\omega)$ and optical reflectivity $R(\omega)$ spectra of Sm_3S_4, as well as the spectra calculated with LSDA, LSDA+U and with the $4f$ electrons in the core. We mention, furthermore, that we have convoluted the calculated spectra with a Lorentzian whose width is 0.4 eV to approximate lifetime broadening. This picture clearly demonstrates that the best description is unambiguously given by the LSDA+U approach. As was mentioned above, the LSDA theory produces a metallic solution and, therefore, gives the wrong asymptotic behavior for the optical reflectivity and the extinction coefficient $k(\omega)$ as $\omega \to 0$. The most prominent discrepancy in the LSDA spectra is the extra peaks between 0 and 1.5 eV in the extinction coefficient $k(\omega)$ caused by interband transitions involving the occupied $4f_{5/2}$ and unoccupied $4f_{7/2}$ hybridized states. In the LSDA+U approach, the empty $4f_{7/2}$ state energies are shifted upward due to the on-site Coulomb interaction U_{eff}. As a result, the transitions involving the unoccupied $4f_{7/2}$ states do not take place at small photon energies, and the erroneous peak structures around 0 to 1.5 eV disappear from the optical spectra.

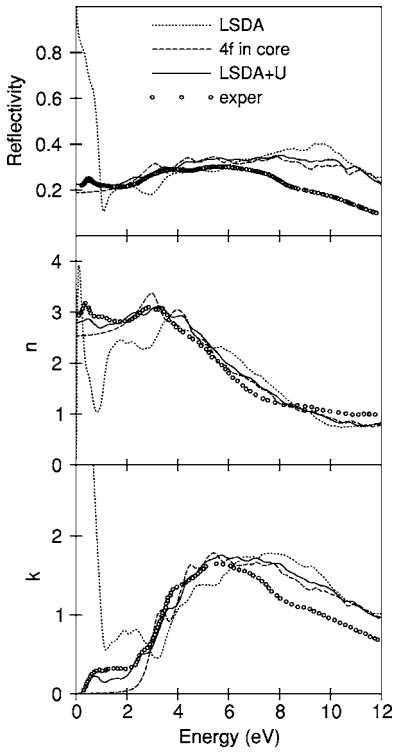

FIG. 10. Calculated optical reflectivity R, real refractive index n and extinction coefficient k of Sm_3S_4 treating $4f$ states as (1) fully localized ($4f$ in core) (dashed line), (2) itinerant (dotted line), and (3) partly localized (LSDA+U approximation) (solid line) compared with experimental data (open circles) (Ref. 32).

The calculations in which the $4f$ electrons are treated as quasicore are able to reproduce correct asymptotic behavior for the optical reflectivity and the refractive index $n(\omega)$ as $\omega \to 0$ similar to the LSDA+U calculations, but, they fail in producing a peak at around 0.6 eV in the refractive index $n(\omega)$ and the extinction coefficient $k(\omega)$. This peak is mostly determined by the interband transitions between occupied $4f_{5/2}$ states hybridized with S p states and two empty $4f_{\text{spin-up}}$ bands situated in close vicinity of the Fermi level.

D. Comparison between Sm_3S_4 and Eu_3S_4

Samarium chalcogenides Sm_3X_4 (X=S, Se, Te) do not exhibit any evidence of charge ordering at low temperature and show a charge glass state due to the random distribution of Sm^{2+} and Sm^{3+} ions.[38] This glass transition of Sm_3X_4 is in strong contrast with the charge ordering of the isomorphic compound Eu_3S_4. In the latter compound, a first-order charge-ordering transition occurs at about 188.5 K, below which the distribution of di- and trivalent cations is no longer random.[43] A microscopic description of the charge ordering and the charge glass states in rare earth chalcogenides is completely lacking. Any detailed model calculations of these phenomena must be based on the knowledge of their electronic and magnetic structures. In this section we compare Sm_3S_4 and Eu_3S_4 compounds in several aspects, namely, their band and magnetic structures, as well as the hybridization effects between the $4f$ and S $3p$ electrons.

TABLE I. The calculated spin M_s, orbital M_l, and total M_t magnetic moments at the rare earth site (in μ_B) of Sm_3S_4 and Eu_3S_4 (low temperature charge-ordered $I\bar{4}2d$ phase).

Ion	Moment	Sm_3S_4	Eu_3S_4
R^{3+}	M_s	4.89	0
	M_l	−4.39	0
	M_t	0.50	0
R^{2+}	M_s	0	6.76
	M_l	0	0.00
	M_t	0	6.82

One should mention that the magnetism of the Eu^{2+} (configuration $4f^7$) and Eu^{3+} (configuration $4f^6$) ions is the reverse of that of the Sm^{2+} ($4f^6$) and Sm^{3+} ($4f^5$) ions, i.e., the trivalent Eu ion has the same magnetic ground state of J=0 as that of the divalent Sm ion. The magnetic ground state of the Eu^{2+} ions is J=7/2 no orbital moment.

Table I lists the calculated spin M_s, orbital M_l, and total M_t magnetic moments (in μ_B) of Sm_3S_4 and Eu_3S_4. The spin and orbital moments are almost equal in Sm_3S_4 and have opposite signs which gives a very small total magnetic moment of $0.5\mu_B$ per ion. Due to its f^7 atomic configuration, Eu^{2+} has no orbital moment.

Figure 11 shows the expanded view of the band structures and total DOS's of Sm_3S_4 and Eu_3S_4 compounds. Both the compounds are semiconductors with an energy gap of 0.25 and 1.70 eV, respectively. The theoretically calculated energy gaps are in complete agreement with the optical measurements.[32,33] The energy gap in Eu_4S_3 is formed by the $4f$ states at the $8d$ sublattice positioned between occupied Eu^{2+}_{8d} states which are strongly hybridized with S $3p$ states and empty Eu^{3+}_{8d} states which cut the very bottom of Eu $5d$ band. The quite small energy gap in Sm_4S_3 also separates the $4f$ bands which belong to divalent and trivalent Sm ions,

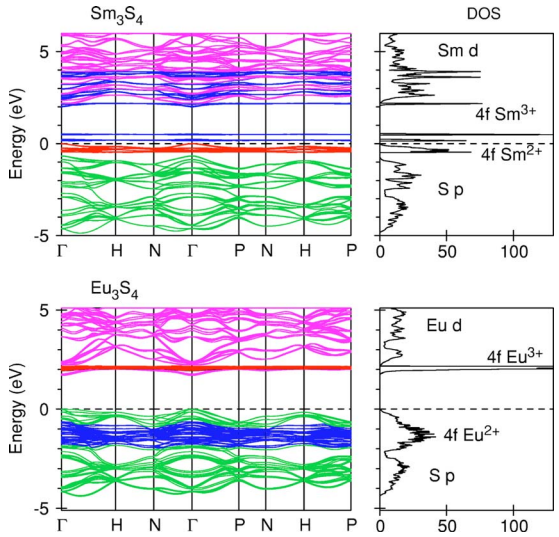

FIG. 11. (Color online) The energy band structure and total DOS [in states/(cell eV)] calculated for Sm_3S_4 and Eu_3S_4 calculated in the LSDA+U approximation.

respectively. In both cases the gap depends on the position of the f states and the choice of U can strongly affect its value, however, we should mention that in our calculations we did not consider the value of U as an adjustable parameter but calculated it using the constrained LSDA approach.[56]

Goto and Lüthi argue[5] that the difference between the charge glass state in Sm_3X_4 (X=S, Se, or Te) and the charge ordering in Eu_3S_4 could be the different hybridization effect of the $4f$ electrons with $3p$ electrons of the chalcogenides.

From the comparison of band structures presented in Fig. 11 we can conclude that the $4f$-$3p$ hybridization effect is really quite different in Eu_3S_4 and Sm_3S_4 compounds. The S $3p$ electrons hybridize with magnetic Eu^{2+} $4f$ electrons in Eu_3S_4 and nonmagentic Sm^{2+} $4f$ electrons in Sm_3S_4. Due to Zeeman splitting the magnetic Eu^{2+} $4f$ states occupy quite a large energy interval inside of the S $3p$ band, strongly hybridized with S $3p$ states. Nonmagnetic Sm^{2+} $4f$ states in Sm_3S_4 cross the very top of S $3p$ band, therefore the $4f$-$3p$ hybridization is expected to be smaller in comparison with the Eu_3S_4 compound.

On the other hand, in Sm_3Se_4 and Sm_3Te_4, nonmagnetic Sm^{2+} $4f$ states are shifted downward from the top of chalcogen $3p$ band. Taking into account that the extension of chalcogen $3p$ valence wave function increases going from the top to the bottom of the band and also going from S to Te one would expect that the $4f$-$3p$ hybridization is increased going from Sm_3S_4 to Sm_3Te_4 through the series. It manifests itself in a width of the Sm^{2+} $4f$ states in these compounds. In Sm_3S_4 Sm^{2+} $4f$ valence states are narrow with a high density of states. There is a hybrization energy gap of about 0.2 eV between Sm^{2+} $4f$ and S $3p$ states. In the case of Sm_3Se_4 and Sm_3Te_4 the Sm^{2+} $4f$ DOS's can hardly be distinguished from chalcogen $3p$ DOS's and the $4f$-p hybridization in these compounds (not shown) is rather similar to the corresponding hybridization in Eu_3S_4 than in Sm_3S_4. Nevertheless, Sm_3Se_4 as well as Sm_3Te_4 show no sign of a phase transition to charge ordering at low temperatures. In lowering the temperature the fluctuations of their $4f$ electrons freeze gradually into a charge glass state similar to Sm_3S_4. Therefore, although the $4f$-$3p$ hybridization effect is quite different in Eu_3S_4 and Sm_3S_4 compounds, it is probably not a main reason for the difference in their ground states.

Seeking the answer to the question why does Sm_3X_4 favor the charge glass state and does not exhibit charge ordering like Eu_3S_4 we performed two numerical experiments. In the first one, by reducing the number of the symmetry operations we make all the atoms in the unit cell nonequivalent and then interchange the places of di- and trivalent Sm and Eu ions. We found that the interchanging of Sm ions with different valency in Sm_3S_4 costs smaller total energy than in the case of interchanging Eu ions in Eu_3S_4. So Sm_3S_4 probably has a larger tendency to charge disorder in comparison with Eu_3S_4.

In the second experiment we tried to check whether the local easy magnetization axes for two nonequivalent pairs of magnetic Sm^{3+} ions in Sm_3S_4 have the same orientation by calculating the total energy as a function of their magnetic moment direction. For simplicity we placed $4f$ electrons of the nonmagnetic Sm^{2+} ion in the core. In order to minimize the contribution of the exchange interaction into the total energy we arranged Sm^{3+} ions in each pair antiferromagnetically, thus, making the exchange energy independent of the relative orientation of the magnetization of the pairs. We found that the magnetic Sm^{3+} ions have different easy magnetization axes defined by the polar angles θ=40°, ϕ=90° and θ=40°, ϕ=0°, for the first and the second Sm^{3+} pair, respectively (θ and ϕ are defined with respect to the [001] direction). In order to verify these results we calculated the dependence of the total energy on the magnetization direction for each Sm^{3+} pair independently. This was achieved by setting the spin-orbit interaction strength at another pair of Sm^{3+} ions to zero, which effectively decouples their magnetic moments from the lattice. The total energy minima were again found for different magnetization directions, close to those mentioned above. It should be pointed out that strong magnetocrystalline anisotropy in Sm_3S_4 prevents collinear magnetic order and may favor the charge glass state in this compound.

The chemical formula involving the information on the valence in Eu_3S_4 is given as $[Eu^{3+}]_{4a}[Eu^{2+}Eu^{3+}]_{8d}(S^{2-})_4$. There is only one type of magnetic Eu^{2+} ion in the unit cell of Eu_3S_4 and two types of nonmagnetic Eu^{3+} ions. Eu^{2+} has no orbital magnetic moment (Table I) and Eu_3S_4 possesses a first order nonmagnetic phase transition near T_{co}=188.5 K,[40,43] as well as phase transition to a ferromagnetic state below T_c=3.8 K.[42] However, a large difference between T_{co} and T_c indicate that the magnetic interactions probably play a minor role for the charge ordering in Eu_3S_4.

The difference in the magnetic structures and the $4f$-$3p$ hybridization effects in Eu_3S_4 and Sm_3S_4 play an important role in determining their ground states properties. However, it is still not clear why Sm_3X_4 favors the charge glass state and does not exhibit charge ordering like Eu_3S_4. This question needs additional theoretical investigation using more sophisticated many-body approaches.

V. SUMMARY

For Sm_4Bi_3, the LSDA+U band structure calculations provide a two-band model of the electronic structure, (1) a wide, nearly fully occupied Bi p valence band and (2) a very narrow, marginally occupied Sm $4f$ band, weakly hybridized with the Bi p band in a small $\mathbf{k}$ space region near the Γ point of the BZ. The mobility of heavy $4f$ electrons is assumed to be negligible in comparison with the mobility of pnictide p electrons. So the transport properties of Sm_4Bi_3 are mostly determined by the number of pnictide p holes. Pressure, doping, etc., may slightly change the relative position of these two bands and hence strongly affect the low carrier density and the transport properties. But the $4f$ shell of the Sm^{3+} ions is little influenced as long as the charge order is maintained.

The most prominent difference in the electronic structure of the Sm_4Bi_3 compound in comparison with the other two samarium pnictides is in the position and occupation of the sixth hole $4f$ spin-up energy level. The pinning of a partly occupied sixth f spin-up level is different in these compounds. If one moves from Sm_4Bi_3 to Sm_4As_3 the peak position of the sixth hole $4f$ spin-up level shifts toward higher energy from the Fermi level. The partial occupation of the sixth hole f level is thus decreasing going from Sm_4Bi_3 to

Sm_4As_3 along with a decrease of the lattice constant. Our results can be considered as qualitative theoretical support of the conclusion derived in Ref. 15, that the Sm^{3+} state is enhanced relative to the Sm^{2+} state from the substitution of Bi ions by Sb ones as well as from the application of pressure in the Sm_4Bi_3.

As classical mixed valence compounds Eu_3S_4 and Sm_3X_4 (X=S, Se or Te) constitute very interesting systems exhibiting unusual behavior due to strong electronic correlations. A detailed comparison between Eu_3S_4 and Sm_3S_4 shows that these two compounds have quite different electronic and magnetic structures as well as different hybridization character of the $4f$ electrons with S $3p$ electrons.

We found that the $4f$-$3p$ hybridization in Sm_3S_4 is expected to be smaller in comparison with the Eu_3S_4 compound. On the other hand, the $4f$-$3p$ hybridization in Sm_3Se_4 and Sm_3Te_4 is closer rather to the corresponding hybridization in Eu_3S_4 than in Sm_3S_4. Nevertheless, Sm_3Se_4 as well as Sm_3Te_4 shows no sign of a phase transition to a charge ordered state at low temperatures. Therefore, the difference in the hybridization in Eu_3S_4 and Sm_3S_4 is probably not a main reason for the difference in their ground states.

Eu_3S_4 and Sm_3S_4 compounds have quite different magnetic structures. Eu^{2+} has no orbital moment. The orbital moment of magnetic Sm^{3+} ions in Sm_3S_4 is quite large and has the opposite direction to the spin moment. We found that easy magnetization axes are different for two nonequivalent Sm^{3+} ions, and the strong local magnetocrystalline anisotropy in Sm_3S_4 might prevent the appearance of the collinear magnetic order in the compound.

In the view of the distribution of valence ions, the low-temperature phase of Eu_3S_4 is similar to the room-temperature phase of magnetite. Di- and trivalent ions are randomly distributed in the B and $8d$ sublattices in Fe_3O_4 and Eu_3S_4, respectively. However, Fe_3O_4 undergoes at T_V=120 K a first-order phase transition (Verwey transition).[11] This phase transition is accompanied by long range charge ordering of Fe^{3+} and Fe^{2+} ions on $B1$ and $B2$ sites of the B sublattice. There are some indications that similar transitions with charge ordering of Eu^{2+} and Eu^{3+} on the $8d$ sublattice may occur also in Eu_3S_4 at low temperatures.[43] However, there are some serious technical difficulties in determining the crystal structure of Eu_3S_4 below T=3.8 K.[43]

In conclusion we would like to point out that the LSDA+U method which combines LSDA with a basically static, i.e., Hartree-Fock-type, mean-field approximation for a multiband Anderson lattice model cannot fully describe such complex phenomena as the charge ordering or the charge glass states in rare earth chalcogenides. However, this method can be considered as the first step toward a better description of strongly correlated electron systems. The LSDA+U method gave a correct insulating ground state solution for Sm and Eu chalcogenides. This method provides the correct energy positions of $4f$ energy bands and gives a reasonable description of the optical properties and XPS spectra in Sm_3S_4.

A detailed investigation of the electronic and magnetic structures of rare earth chalcogenides presented in this paper should be regarded as a step toward more sophisticated model calculations of the charge ordering and the charge glass state phenomena.

There are several computational methods which go beyond the LDA or LDA+U approach in the treatment of ground states and excited states of correlated electron materials. These methods include the self-interaction correction (SIC) approach, dynamical mean-field theory (DMFT), and the GW approximation. Although they are more computationally demanding, it would be of interest to investigate their applicability to the materials and phenomena discussed in this work.

ACKNOWLEDGMENTS

The authors would like to thank Professor Peter Fulde for reading the paper and fruitful discussions. This work was carried out at the Max Planck Institute for the Physics of Complex Systems and Ames Laboratory, which is operated for the U.S. Department of Energy by Iowa State University under Contract No. W-7405-82. This work was supported by the Office of Basic Energy Sciences of the U.S. Department of Energy. This work was supported by the CRDF program Contract No. 14589. V.N. Antonov gratefully acknowledges the hospitality at the Max Planck Institute for the Physics of Complex Systems and Ames Laboratory during his stays.

*Email address: antonov@imp.kiev.ua; antonov@ameslab.gov; Permanent address: Institute of Metal Physics, Vernadsky Street, 03142 Kiev, Ukraine.

[1] C. M. Varma, Rev. Mod. Phys. **48**, 219 (1976).

[2] J. M. Lawrence, P. S. Riseborough, and R. D. Parks, Rep. Prog. Phys. **44**, 1 (1981).

[3] P. Wachter, in *Handbook of the Physics and Chemistry of Rare Earths*, edited by K. A. Gschneidner, L. Eyring, and S. Hüfner (North-Holland, Amsterdam, 1994), Vol. 19, p. 177.

[4] V. Antonov, B. Harmon, and A. Yaresko, *Electronic Structure and Magneto-Optical Properties of Solids* (Kluwer Academic, Dordrecht, Boston, London, 2004).

[5] T. Goto and B. Lüthi, Adv. Phys. **52**, 67 (2003).

[6] V. N. Antonov, B. N. Harmon, and A. N. Yaresko, Phys. Rev. B **63**, 205112 (2001).

[7] V. N. Antonov, B. N. Harmon, and A. N. Yaresko, Phys. Rev. B **66**, 165208 (2002).

[8] V. N. Antonov, B. N. Harmon, and A. N. Yaresko, Phys. Rev. B **66**, 165209 (2002).

[9] V. N. Antonov, M. Galli, F. Marabelli, A. N. Yaresko, A. Y. Perlov, and E. Bauer, Phys. Rev. B **62**, 1742 (2000).

[10] P. Fulde, Ann. Phys. (N.Y.) **6**, 178 (1997).

[11] E. J. Verwey and P. Haayman, Physica (Amsterdam) **8**, 1979 (1941).

[12] V. N. Antonov, B. N. Harmon, V. P. Antropov, A. Y. Perlov, and A. N. Yaresko, Phys. Rev. B **64**, 134410 (2001).
[13] I. Leonov, A. N. Yaresko, V. N. Antonov, M. A. Korotin, and V. I. Anisimov, Phys. Rev. Lett. **93**, 146404 (2004).
[14] K. Neumaier, K. Andres, and H. R. Ott, Physica B & C **108**, 1343 (1981).
[15] A. Ochiai, T. Suzuki, and T. Kasuya, J. Magn. Magn. Mater. **52**, 13 (1985).
[16] A. Ochiai, D. X. Li, Y. Haga, O. Nakamura, and T. Suzuki, Physica B **186–188**, 437 (1993).
[17] J.-X. Boucherle, F. Givord, J. Schweizer, J.-M. Mignot, E. Lelievre-Berna, H. Aoki, and A. Ochiai, Physica B **267–268**, 47 (1999).
[18] A. Ochiai, Y. Sima, and M. Shirakawa, J. Phys. Soc. Jpn. **72**, 3174 (2003).
[19] P. Fulde, B. Schmidt, and P. Thalmeier, Europhys. Lett. **31**, 323 (1995).
[20] M. Kohgi *et al.*, Physica B **230–232**, 638 (1997).
[21] A. Jayaraman, R. G. Maines, and E. Bucher, Solid State Commun. **27**, 709 (1978).
[22] H. Aoki, A. Ochiai, and T. Suzuki, Physica B **259–261**, 349 (1999).
[23] S. Suga, Phys. Scr. **17**, 228 (1987).
[24] S. Suga, A. Sekiyama, S. Imada, T. Suzuki, H. Aoki, and A. Ochiai, Physica B **281–282**, 158 (2000).
[25] F. Hulliger, Mater. Res. Bull. **14**, 33 (1979).
[26] G. Worman, E. V. Sampathkumaran, and G. Kaindal, J. Magn. Magn. Mater. **54–57**, 338 (1986).
[27] F. L. Carter, J. Solid State Chem. **5**, 300 (1972).
[28] M. Picon, L. Domange, J. Flahaut, M. Guittard, and M. Patrie, Bull. Soc. Chim. Fr. **2**, 221 (1960).
[29] E. Bucher, K. Andres, F. J. di Salvo, J. P. Maita, A. C. Gossard, A. S. Cooper, and G. W. Hull, Phys. Rev. B **11**, 500 (1975).
[30] B. Batlogg, E. Kaldis, A. Schlegel, and P. Wachter, Phys. Rev. B **14**, 5503 (1976).
[31] A. Tamaki, T. Goto, M. S. S. Kunii, T. Suzuki, T. Fujimura, and T. Kasuya, J. Magn. Magn. Mater. **31–34**, 383 (1983).
[32] B. Batlogg, E. Kaldis, A. Schlegel, G. von Schulthess, and P. Wachter, Solid State Commun. **19**, 673 (1976).
[33] P. Wachter, Philos. Mag. B **42**, 497 (1980).
[34] H. Goto, K. Baba, T. Goto, S. Nakamura, A. Tamaki, A. Ochiai, T. Suzuki, and T. Kasuya, J. Phys. Soc. Jpn. **62**, 1365 (1993).
[35] J. M. D. Goey, B. Cornut, F. Holtzberg, and S. von Molnar, J. Appl. Phys. **50**, 1923 (1979).
[36] P. A. Alekseev, J.-M. Mignot, R. Kahn, A. Ochiani, E. S. Clementyev, V. N. Lazukov, E. V. Nefeodova, I. P. Sadikov, and P. Fabi, J. Phys.: Condens. Matter **12**, 2725 (2000).
[37] S. Takagi, H. Suzuki, A. Ochiai, and T. Suzuki, J. Phys. Soc. Jpn. **62**, 2861 (1993).
[38] A. Tamaki, T. Goto, S. Kunii, T. Suzuki, T. Fujimura, and T. Kasuya, J. Phys. C **18**, 5849 (1985).
[39] T. Tayama, K. Tenya, H. Amitsuka, T. Sakakibara, A. Ochiai, and T. Suzuki, J. Phys. Soc. Jpn. **65**, 3467 (1996).
[40] R. Pott, G. Güntherodt, W. Wichelhaus, M. Ohl, and H. Bach, Phys. Rev. B **27**, 359 (1983).
[41] F. Holtzberg, Philos. Mag. B **42**, 491 (1980).
[42] E. Görlich, H. U. Hrynkiewicz, R. Kmiec, K. Latka, and K. Tomala, Phys. Status Solidi B **64**, 147 (1974).
[43] H. Ohara, S. Sasaki, Y. Konoike, T. Toyoda, K. Yamawaki, and M. Tanaka, Physica B **350**, 353 (2004).
[44] T. Suzuki, Physica B **186–188**, 347 (1993).
[45] M. Sugita, S. Kunii, K. Takegahara, N. Sato, T. Sakakibara, P. J. Markowski, M. Fujioka, M. Date, and T. Kasuya, in *Crystalline Electric Field Effects in f-electron Magnetism*, edited by R. P. Guertin, W. Suski, and Z. Zolnierek (Plenum, New York, 1982), p. 479.
[46] S. Takagi, T. Suzuki, A. Amato, F. N. Gygax, A. Schenk, and A. Ochiai, Hyperfine Interact. **104**, 151 (1997).
[47] U. Ahleim, K. Fraas, P. H. P. Reinders, F. Steglich, D. Nakamura, T. Suzuki, and T. Kasuya, J. Magn. Magn. Mater. **108**, 213 (1992).
[48] P. Villars and L. D. Calvert, *Pearson's Handbook of Crystallographic Data for Intermetallic Phases* (ASM International, Materials Park, OH, 1991).
[49] M. O'Keeffe and S. Andersson, Acta Crystallogr., Sect. A: Cryst. Phys., Diffr., Theor. Gen. Crystallogr. **A33**, 914 (1977).
[50] O. K. Andersen, Phys. Rev. B **12**, 3060 (1975).
[51] V. V. Nemoshkalenko, A. E. Krasovskii, V. N. Antonov, V. N. Antonov, U. Fleck, H. Wonn, and P. Ziesche, Phys. Status Solidi B **120**, 283 (1983).
[52] U. von Barth and L. Hedin, J. Phys. C **5**, 1629 (1972).
[53] P. E. Blöchl, O. Jepsen, and O. K. Andersen, Phys. Rev. B **49**, 16223 (1994).
[54] V. I. Anisimov, J. Zaanen, and O. K. Andersen, Phys. Rev. B **44**, 943 (1991).
[55] A. N. Yaresko, V. N. Antonov, and P. Fulde, Phys. Rev. B **67**, 155103 (2003).
[56] V. I. Anisimov and O. Gunnarsson, Phys. Rev. B **43**, 7570 (1991).
[57] V. N. Antonov, A. N. Yaresko, A. Y. Perlov, P. Thalmeier, P. Fulde, P. M. Oppeneer, and H. Eschrig, Phys. Rev. B **58**, 9752 (1998).
[58] B. Schmidt *et al.*, Physica B **300**, 123 (2001).
[59] R. D. Shannon and C. T. Prewitt, Acta Crystallogr., Sect. B: Struct. Crystallogr. Cryst. Chem. **B25**, 925 (1969).
[60] O. Berkooz, M. Malamud, and S. Shtrikman, Solid State Commun. **6**, 185 (1968).
[61] Y. Fujii, G. Shirane, and Y. Yamada, Phys. Rev. B **11**, 2036 (1975).
[62] T. Toyada, S. Sasaki, and M. Tanaka, Jpn. J. Appl. Phys., Part 1 **36**, 2247 (1997).
[63] M. Campagna, G. K. Wertheim, and E. Bucher, *Structure and Bonding* (Springer, Berlin, 1976), Vol. 30.
[64] M. Campagna, E. Bucher, G. K. Wertheim, and L. D. Longinotti, Phys. Rev. Lett. **33**, 165 (1974).
[65] J. J. Yeh and I. Lindau, At. Data Nucl. Data Tables **32**, 1 (1985).
[66] M. Campagna, E. Bucher, G. K. Wertheim, D. N. E. Buchanan, and L. D. Longinotti, Phys. Rev. Lett. **32**, 885 (1974).
[67] P. A. Cox, *Structure and Bonding* (Springer, Berlin-Heidenberg-New York, 1975), Vol. 24.
[68] G. Racah, Phys. Rev. **76**, 1352 (1949).